Nonlinear wave propagation through multiple scattering media and virtual time reversal focusing

Gonzalo Garay,[1] Nicolás Benech,[1] Yamil Abraham,[1] and Carlos Negreira[1]

Laboratorio de Acústica Ultrasonora, Inst. de Física, Fac. de Ciencias, Montevideo, Uruguay

(Dated: 2 August 2020)

In this work, the propagation of an ultrasonic nonlinear wave through a multiple scattering medium is experimentally studied. The interaction between multiple scattering and nonlinear phenomena is analyzed by the cross correlation of the scattered field. This approach corresponds to a virtual time reversal. The cross correlated field is focused in both time and space. In linear regime, it is known that the focal width decreases as the thickness of the multiple scattering medium is increased. In this work, it is shown that this behavior is followed by a nonlinear wave and its harmonics. Moreover, due to the spectral richness of the nonlinear wave, the focal width is reduced in the nonlinear regime. This fact allows concluding that the harmonics propagate following a linear scattering equation, although a nonlinear regime is required to generate them. Beside the experimental work, an estimation of the order of magnitude of the parameters that quantify nonlinearity and scattering phenomena is performed. The estimation shows that the Lighthill-Westervelt equation is as an accurate theoretical model for describing the multiple scattering of a nonlinear wave in the experiments.

I. INTRODUCTION

The scattering phenomena are an important subject in acoustics. From metal crack detection to imaging in medicine, wave propagation in non-homogeneus media becomes an important topic on non-invasive techniques[1]. Some studies on multiple scattering of ultrasonic waves were carried out on two-dimensional media, consisting of a random collection of parallel rods submerged in water[2,3]. This kind of media can be easily assembled and its construction allows changing some parameters (as the thickness or the scatterers density) in a simple way. Moreover, a single configuration of disorder as well as an ensemble average (coherent wave) of acoustic waves can be studied. A reference work was published by A. Tourin et al., where some experimental methods to characterize a two-dimensional sample in terms of transport parameters are described[3]. In their paper, the authors describe an experiment to measure the coherent field of a scattered wave. This measure allows computing the elastic mean free path, parameter related to the density of scatterers and their cross section. A similar procedure was followed by N. Viard et al. to study the interaction of a shock wave with a multiple scattering medium[4]. Nonlinear waves have a particular characteristic: the generation of harmonics. This implies that a wave with central frequency f_0 will generate, as it propagates, spectral components at frequencies multiples of f_0. Taking this into account, Viard et al. studied the coherent field of a nonlinear wave which traverses a multiple scattering medium. The authors measured the elastic mean free path of the spectral components present in the wave. They conclude that, under their experimental conditions, both nonlinear phenomena and multiple scattering phenomena do not interact.

The estimation of the coherent field implies an average of the acoustic field over different configurations of disorder (ensemble average). In this work, an alternative approach is proposed. The whole wave -including the coda wave- is studied by the cross correlation of the field which has traversed a single configuration. This procedure corresponds to a virtual time reversal.

The time reversal process has been widely studied and applied in various acoustical systems. In the linear regime, it has been studied by M. Fink since the 90's[5,6]. The time reversal process is able to focus the acoustic energy in both space and time. This property allows getting very high amplitude focused waves when is applied to devices like waveguides[7] or resonant cavities[8,9]. Moreover, the time reversal process is able to focus waves through multiple scattering media. In a linear regime, it was shown that the focal spot width decreases the greater the thickness of the medium[10].

In a nonlinear regime, the time reversal process in a homogeneous medium has been studied experimentally by M. Tanter et al.[11], showing that a nonlinear wave is invariant under a time inversion if it propagates a distance lower than the distance where the shock wave occurs. In their work, the authors point out the difficulty of carrying out the experiment because the acoustic energy of a nonlinear wave is distributed into harmonics. Therefore, a device with very large bandwidth is required. Piezoelectric transducers are unable to properly emit the higher harmonics. Therefore, the authors figured out an experimental setup, which implies the reflection of waves to avoid the re-emission of the reversed wave from the transducer.

The difficulty pointed out by Tanter et al. can be avoided by performing a virtual time reversal process, because the harmonics are present in the cross correlated field. Then, we proceed in this way to analyze the coupling between nonlinear and scattering phenomena. The main point of the work is centered on determining the spatial focal width at -3 dB as a function of the thickness of the multiple scattering medium. The results obtained are compared with already known results of the linear theory and the behavior of the harmonics present in the scattered wave is characterized. The work is organized as follows: in section II the experimental setup together with the features of the multiple scattering medium are described and in section III an appropriate theoretical model of scattering for the experiments is briefly described. Then, based on the estimation of the orders of magnitude of the parameters involved, a conclusion about the interaction between scattering and nonlinearity is sketched out. The theoretical approach is verified experimentally from section IV. In this section, the characteristics that evidence the nonlinear regime of the scattered waves are presented. Those are: the generation of harmonics, typical nonlinear phenomenon and their presence in the coda signal, characteristic of the multiple scattering. Moreover, a study of the coherent field, the harmonics present in it and its interaction with multiple scattering is presented. The results gave us the motivation for performing a different experiment involving the whole wave and not only the coherent field: the virtual time reversal, which is presented in section V.

II. EXPERIMENTAL SETUP

The experiments of this work are carried out over the setup shown in figure 1. A multiple scattering medium is positioned between a flat circular transducer (nominal diameter $\phi = 28.757\,\mathrm{mm}$, central frequency $f_0 = 1\,\mathrm{MHz}$) and a needle hydrophone (Onda HNA-0400) immersed in degassed water (sound speed $c_w = 1.5\,\mathrm{mm}\,\mu\mathrm{s}^{-1}$ and density $\rho_w = 1.00\,\mathrm{g}\,\mathrm{cm}^{-3}$). The degassing process avoid the formation of cavitation bubbles. The transducer is excited with five cycles of a 1 MHz sinusoidal signal generated with a function generator (Tektronix AFG 3021B) and magnified through a 50 dB gain RF power amplifier (E&I A075). The amplitude of the output voltage from the amplifier varies between 32 V and 285 V. This amplitude is referred to as *applied voltage* and is noted as V_{in}. The hydrophone is placed

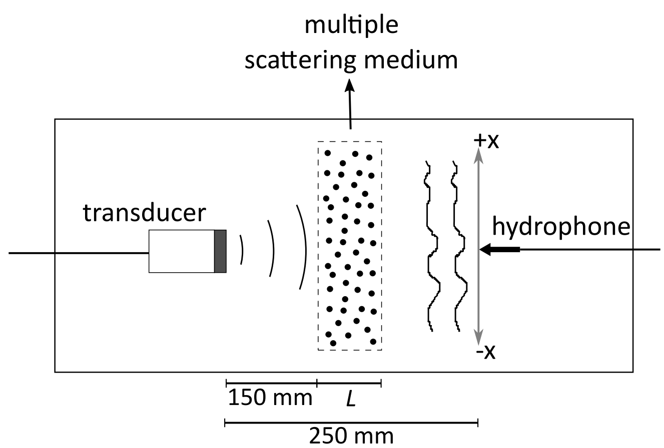

FIG. 1. The system consists of a transducer and a hydrophone immersed in water and 250 mm apart. Between them (at 150 mm from the transducer) is placed a multiple scattering medium of thickness L composed of randomly distributed vertical copper rods. The transducer is excited with a five-cycle sinusoidal signal at 1 MHz. The generated wave is acquired by the hydrophone at positions along the x-axis.

250 mm far from the transducer and with a stepper motor (minimum step 0.254 mm) it is positioned at different points in the x-axis defined in figure 1. In the position $x = 0$ the hydrophone is in front of the transducer.

The multiple scattering medium is a slab composed of parallel copper cylinders (sound speed $c_c = 3.6\,\mathrm{mm}\,\mu\mathrm{s}^{-1}$ and density $\rho_c = 8.96\,\mathrm{gcm}^{-3}$), nominal diameter 0.7 mm and effective length 120 mm. The cylinders are randomly positioned on a grid of length 140 mm (measured parallel to the x-axis) and thickness L, where the minimum distance between two cylinders is 2.5 mm. Of the available grid points, three quarters are filled with cylinders. With this configuration, the ratio between the area occupied by the cylinders and the total area occupied by the slab is, on average, $a_c = 0.0462$, while the ratio between the area occupied by water and the total area is $a_w = 0.9538$. The experiments are performed by changing the thickness of the slab between $L = 8\,\mathrm{mm}$ and $L = 60\,\mathrm{mm}$.

Experimentally, we found that the maximum pressure amplitude of the fundamental frequency is reached at a distance of 130 mm far from the transducer, while the maximum pressure amplitude of the second harmonic frequency (generated by nonlinear effects) is reached at 180 mm. With this data, it is convenient to place the multiple scattering medium at a distance of 150 mm from the transducer where the first and second harmonics reach a high amplitude (less than 1 dB below their respective maximum level).

The Mach number ϵ is useful to quantify the order of magnitude of nonlinear phenomena. This number results from the ratio between the particular velocity of the wave on the surface of the source and the propagation speed. Assuming that the pressure p_s and the velocity v_s on the source surface are related as $p_s = c_0\rho_0 v_s$, the Mach number can be obtained as

$\epsilon = \frac{p_s}{\rho_0 c_0^2}$. With a measurement of the acoustic field at 130 mm far from the transducer (where the maximum pressure amplitude is reached) and assuming that the pressure in the transducer face is half this value (as in the linear field of a circular aperture[12]), the order of ϵ can be estimated. For $V_{in} = 32\,\mathrm{V}$ the order of ϵ is 10^{-6} and for $V_{in} = 285\,\mathrm{V}$ the order is 10^{-5}. The Mach number is also useful to estimate the shock formation distance l_s where a plane wave turns into a shock wave, related to the wave number k and the nonlinear parameter β as $l_s = (\beta k \epsilon)^{-1}$. Taking $\beta = 3.5$ for water[4], the shock distance is in the order of magnitude of 10^3 mm, far away from the free propagation distances of the wave (250 mm).

III. THE SCATTERING MODEL. A SIMPLE THEORETICAL APPROACH.

In this work, the interaction between the nonlinear wave and the multiple scattering medium is studied experimentally. However, some properties can be inferred from a theoretical model. Nonlinear scattering phenomena in a non disipative media can be modeled by the generalized Lighthill-Westervelt equation[13]:

$$\left(\nabla^2 - \frac{1}{c_0^2}\frac{\partial^2}{\partial t^2}\right) p - \frac{\nabla \rho_0}{\rho_0} \cdot \nabla p = -\frac{\beta}{\rho_0 c_0^4}\frac{\partial^2 p^2}{\partial t^2} \tag{1}$$

where p represents the acoustic pressure, $c_0 = c_0(\mathbf{r})$ and $\rho_0 = \rho_0(\mathbf{r})$ are the wave speed and the medium density, respectively. The last two magnitudes have a spatial dependence due to the inhomogeneities introduced by the slab. The parameter $\beta = \beta(\mathbf{r})$ quantifies the nonlinearity of the propagation medium and also depends on the spatial coordinate.

The validity of equation 1 requires some hypothesis about the order of magnitude of the variables involved. On one hand, the order of magnitude of nonlinear phenomena can be quantified through the square of the Mach number defined in II. On the other hand, multiple scattering phenomena are of the order of[13]

$$\eta = \left| \frac{c_0 - \bar{c}_0}{\bar{c}_0} \right| \tag{2}$$

where $\bar{c}_0$ is the spatial average of the propagation speed. Finally, equation 1 is valid if the product $\eta\epsilon^2$ is much smaller than η and ϵ^2.

In section II, the sound speed of water and copper together with the ratios a_c and a_w were given. Considering these values, an average speed $\bar{c}_0$ can be computed as $\bar{c}_0 = a_c c_c + a_w c_w$. With this calculation and the equation 2 where c_0 is substituted by c_w, the order of magnitude for the scattering phenomena yields $\eta \approx 10^{-2}$. Therefore, the order of $\eta\epsilon^2$ is 10^{-12}, wich means that the system verifies the hypotheses required by the theoretical model.

An observation can be made based on the estimated orders of magnitude. The wave initially propagates 150 mm in water. In this path, the wave propagation is described by the usual Westervelt equation ($\frac{\nabla\rho_0}{\rho_0} = 0$ in equation 1). The nonlinear propagation implies the generation of harmonics of higher order than the fundamental. When the nonlinear wave impinges the multiple scattering medium, the order of η is greater than ϵ^2. This allows to neglect the term on the right side in equation 1 and the propagation of the wave in the slab is described by a linear scattering equation. This fact suggest that the harmonics propagate following a linear scattering equation, regardless if they have been generated by nonlinear effects or not. This shows that there is no interaction between nonlinear phenomena and multiple scattering. In this case, it is said that these phenomena are decoupled. In sections IV and V, an experimental analysis is performed, which allows to contrast this theoretical statement.

IV. THE NONLINEAR SCATTERED WAVE

A. Harmonics in the coda wave

The properties of the nonlinear scattered waves are analyzed by measuring the acoustic wavefield at $x = 0$. These measurements are shown in figure 2. The scattered waves of figures 2a and 2b, traverse slabs of thicknesses $L = 38$, $15\,\mathrm{mm}$, respectively, and they were acquired by exciting the transducer with $V_{in} = 285\,\mathrm{V}$ ($\epsilon \approx 10^{-5}$). These waves have a longer

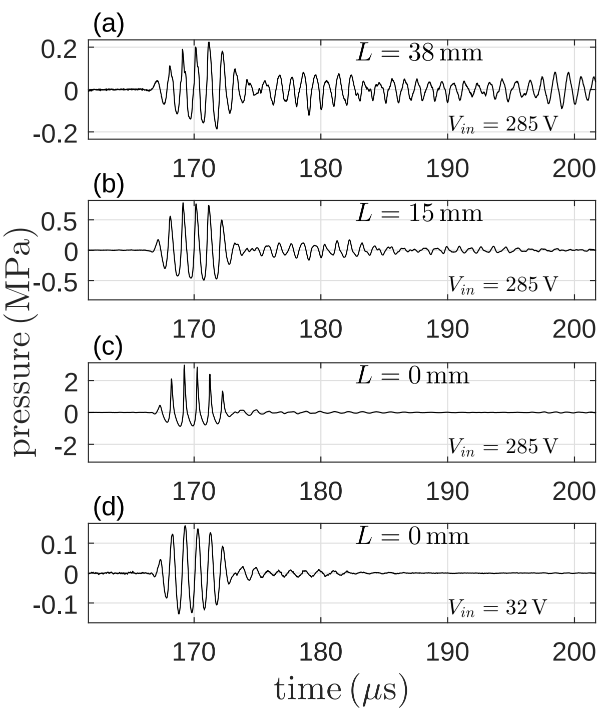

FIG. 2. Temporal waveforms acquired at $x = 0$. The waves traverse slabs of (a) $L = 38\,\mathrm{mm}$, (b) $L = 15\,\mathrm{mm}$ and (c) $L = 0\,\mathrm{mm}$ (the latter is not scattered). The voltage amplitude is $V_{in} = 285\,V$. (d) Non scattered wave acquired with $V_{in} = 32\,V$. As L increases the shock-wave trace is less noticeable. The same happens with a lower voltage amplitude ($V_{in} = 32\,V$).

duration than the initial excitation ($5\,\mu s$), because part of them are delayed by multiple reflections that occurs in the slab. This part is known as the *coda wave*[2,3]. The wave in figure 2c is not scattered ($L = 0$) and it was acquired with the same voltage. It exhibits a shock-wave trace due to the nonlinear harmonics of higher order than the fundamental one. The non-scattered linear wave of figure 2d, acquired with $V_{in} = 32\,\mathrm{V}$ ($\epsilon \approx 10^{-6}$) do not show this trace. Moreover, this trace disappears progressively if the thickness of the slab is increased. To better understand this fact, the spectra of the nonlinear waves are shown in figure 3a. The intensity level is represented in a dB scale computed from the spectral amplitude obtained from a FFT algorithm. The reference (0 dB) is the maximum level of the spectrum of the non scattered wave (around 1 MHz). The waves have a spectral component at the central frequency (1 MHz) but also exhibits the components at the frequencies of its harmonics. Although the harmonics are recognizable in the three signals, the intensity level of each harmonic decreases when the slab is introduced. Moreover, the level of the harmonics decays respect to the fundamental one with each slab, causing the loss of the shock-wave trace pointed before. For example, the difference of the intensity level between the fundamental harmonic and the second one is of 5 dB without the slab and increases to 15 dB for the 38 mm thickness slab.

The harmonics contained in the coda waves of figure 2, can be better analyzed by including the time variable, as was done in the spectrograms of figures 3b to 3d. They were computed by splitting the whole signal into Hamming windows of $5\,\mu$s and performing a FFT. The color scale of the images is in dB, being the reference the maximum amplitude obtained in each spectrogram. In figure 3d, where there is no scattering, the harmonics are concentrated

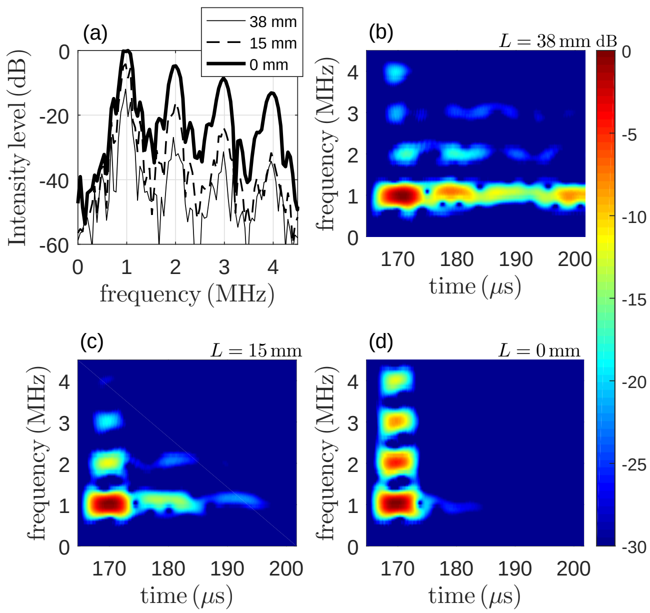

FIG. 3. Color online. (a) Spectra of the waves that traverse slabs of thickness 38 mm (thin line), 15 mm (dashed line) and a non scattered wave (thick line). For the three cases, different harmonics are presented in the wave, but they show a significant decay as the thickness of the slab is increased. (b) Spectrogram of the wave that traverses a 38 mm thickness slab. (c) Spectrogram of the wave that traverses a 15 mm thickness slab. (d) Spectrogram of the non scattered wave. The maximum amplitude of the harmonics in the non-scattered wave are concentrated at the arrival time. As the slab thickness is increased, the harmonics spread into the coda wave.

around 170 μs (arrival time). With a slab of thickness $L = 15\,\mathrm{mm}$ (fig. 3c), the fundamental harmonic and the second harmonic spreads over the coda wave and, with a 38 mm thickness slab (fig. 3b), the third harmonic is also seen spreading over the coda wave.

The measurements presented in this section, show that the high amplitude of the waves can generate nonlinear effects, even if they traverse the multiple scattering medium. Furthermore, the harmonics spread over the coda wave. Then, the multiple scattering has an effect over the nonlinear harmonics. The experimental study of this effect begins in the next subsection by first studying the coherent field of the wave.

B. The coherent wave

The coherent field is studyied by reproducing the Viard's experiment[4]. The spectrum of the coherent field is computed and the level of the harmonics are analyzed as a function of L. In a linear regime, the intensity level (in a dB scale) of the spectral components should decay linearly as $-L/l_e$, where l_e is the elastic mean free path, a frequency-dependent parameter[3].

An estimation of the coherent field is performed by averaging signals acquired in different disorder configurations[3,4]. To achieve this, the position of the slab is changed 0.762 mm parallel to $x-$axis. In this way, 80 signals are recorded for averaging (avoiding being close to the border of the slab).

In figure 4a, the intensity level of the first harmonic is plotted in a dB scale (being the reference the amplitude of its harmonic at $L = 0$) against L. Two data series are compared: with $V_{in} = 32\,V$, where a linear regime can be considered ($\epsilon \approx 10^{-6}$) and with $V_{in} = 285\,V$, where the regime is non linear ($\epsilon \approx 10^{-5}$). Notice that, in both cases, the intensity level decreases linearly as the slab thickness increase. In addition, by performing a linear fitting, the elastic mean free path is calculated in each case. The values obtained are (9.72 ± 0.34) mm in linear regime and (9.90 ± 0.33) mm in nonlinear regime. Taking into account the uncertainty, these values are equal with each other. In a similar way the amplitude of the second harmonic is studied. In figure 4b the decay of its intensity level is plotted against L. The nonlinear data was obtained with a voltage $V_{in} = 285\,\mathrm{V}$. As can be seen in the figure, its intensity level also decreases linearly with L. In linear regime the measure can not be achieved with this system. Instead, the transmitter is changed by a low-power transducer whose central frequency is 2.25 MHz and its bandwidth has a good response at 2 MHz. By exciting the transducer with a 2 MHz signal, a linear decay is

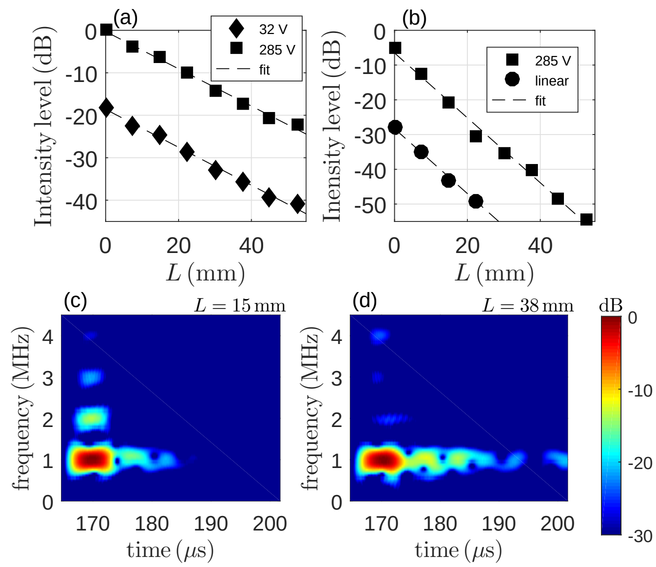

FIG. 4. Color online. (a) Intensity level in dB of the fundamental harmonic of the coherent wave as a function of L. For $V_{in} = 32\,V$ (diamonds) the the regime is linear and for $V_{in} = 285\,V$ (squares), nonlinear. (b) Intensity level of the second harmonic of the coherent wave against L. The circles represent the intensity level of the wave emmitted by a linear transducer at 2 MHz. The dotted line is a linear fit on each data set. (c) Spectrogram of the coherent field of a nonlinear wave that is scattered by a 15 mm thickness slab. (d) The same for a wave scattered by a 38 mm thickness slab. The fundamental frequency spreads over the coda wave but the harmonics are located around the arrival time ($170\,\mu s$).

observed. Moreover, the elastic mean free path is the same in nonlinear regime and in linear regime: (4.65 ± 0.16) mm and (4.65 ± 0.10) mm, respectively.

From these results, it can be concluded that, despite the presence of a nonlinear regime, the first and second harmonics of the coherent wave propagate independently from each other, as happens in a linear regime. However, the harmonics that spread over the coda wave are not considered. It can be noticed from the spectrograms computed for the coherent wave. In figures 4c and 4d, the spectrograms for $L = 15$, $38\,\mathrm{mm}$ with $V_{in} = 285\,\mathrm{V}$, are shown. Unlike those shown in IV A, the harmonics are mainly concentrated around $170\,\mu s$. This fact leads to wonder if the incoherent wave and its harmonics, also propagates as in a linear regime. With this question in mind, we perform a virtual time reversal approach, which include the harmonics of both the coherent and the incoherent wave.

V. THE VIRTUAL TIME REVERSAL APPROACH

There are different ways to describe the time reversal process. In this work, a description based in a linear time-invariant system is presented. Let's $s\,(x, t)$ be the wavefield at the x-axis and let's choose $x = 0$ as the focal position. On one hand, the *real time reversal* process consists on time reversing and re-emitting the signal $s\,(0, t)$. Then, a focused wave at $x = 0$ is achieved. On the other hand, the *virtual time reversal* process consists on computing the following cross correlation:

$$\gamma_c\,(x, t) = s\,(x, t) \star s\,(0, t) \tag{3}$$

where $\gamma(x,t)$ is the cross correlated field. This procedure approaches to a real time reversal process if the signal emitted form the transducer is a very short signal, being the parity of $\gamma(x,t)$ the same of $e(t)$[14].

The operation proposed in equation 3 was performed by measuring the acoustic field on the x-axis and sweeping between $x = -10\,\mathrm{mm}$ and $x = +10\,\mathrm{mm}$. Then, the field $\gamma_c(x,0)$ is computed. Its envelope is shown in a dB color-scale (where the reference is the maximum amplitude) in figures 5a, 5b and 5c for $L = 15$, 38, 60 mm, repectively. The voltage was

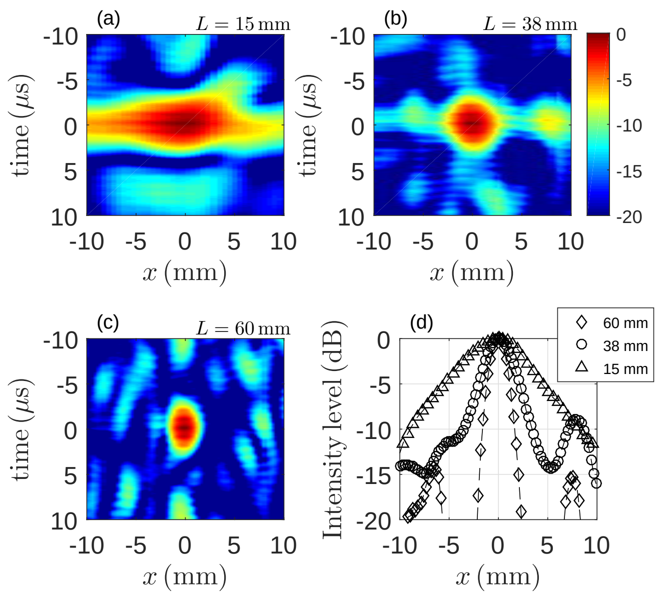

FIG. 5. Color online. Space-time distribution of the acoustic intensity level (in dB) of the virtual time reversal signal obtained with slabs of thicknesses (a) 15 mm, (b) 38 mm and (c) 60 mm. As the images show, the focal width decreases as L increases. (d) Intensity level in dB of $\gamma_c(x,0)$ obtained with slabs of thicknesses 15 mm (triangle), 38 mm (circle) and 60 mm (diamond). The -3 dB focal widths decrease as the thickness of the multiple scattering medium is increased. $V_{in} = 285\,\mathrm{V}$ for each acquisition.

$V_{in} = 285\,\mathrm{V}$. The time scale is shifted in such a way that the focal time is $t = 0$. It is clear that the wave is focused in both time and space. In addition, it can be noticed that the focal width is reduced as the thickness of the slab is increased. This occurs due to the loss of correlation between the spectral components of $s\,(0, t)$ and $s\,(x \neq 0, t)$ as a consequence of the multiple scattering. This result is well known in the linear wave theory[10]. However, here it is shown for nonlinear waves. In figure 5d the intensity level of the cross correlated field is plotted at $t = 0$. The narrowing of the focal spot can be quantified by measuring the width Δx at $-3\,\mathrm{dB}$. For a slab 15 mm thick, the focal width is 7.1 mm and, for a thickness of 60 mm, it reduces to 1.8 mm.

The fundamental and the second harmonics of γ_c are also studied along the $x-$axis to evaluate how the presence of the second harmonic affects the cross correlated field. Considering a window of $5\,\mu\mathrm{s}$ (5 cycles) around $t = 0$, the spectrum of each signal is computed by a FFT algorithm. Figures 6a and 6b show the intensity level of these harmonics in a dB scale (taking as reference the maximum of each data series). The focal width of the first harmonic Δx_1 (fig. 6a) is reduced from 7.5 mm to 1.9 mm as the thickness of the slab is increases from 15 mm to 60 mm. Moreover, the focal width of the second harmonic Δx_2 (fig. 6b) is reduced from 5.6 mm to 1.0 mm. In figure 6c, Δx, Δx_1 and Δx_2 are plotted as a function of L. Notice that for a given thickness L, it is satisfied that $\Delta x_2 < \Delta x < \Delta x_1$. This is clearly observed for $L = 8\,\mathrm{mm}$, but remains true in the whole range studied (although is harder to perceive in the figure).

The observation of the last paragraph shows that the second harmonic, and therefore the nonlinearity, contributes to reduce the focal width. To analyze this fact, the experiment

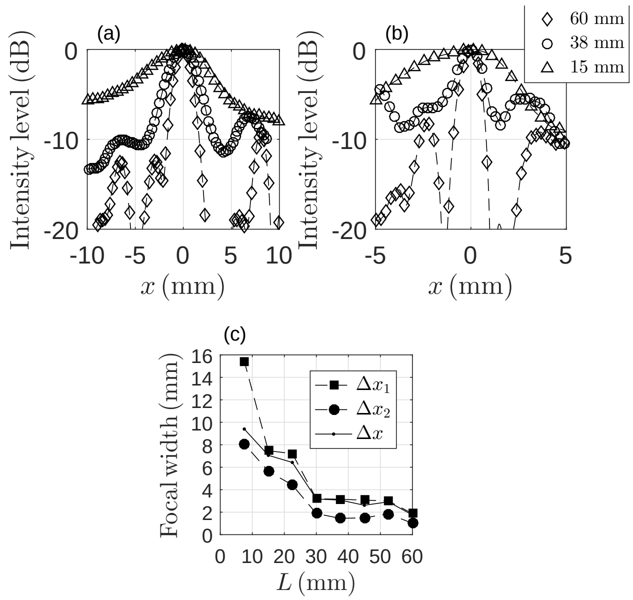

FIG. 6. Intensity level in dB of (a) the first harmonic and (b) the second harmonic at $t = 0$. (c) -3 dB focal width of the first and second harmonic (Δx_1 and Δx_2, respectively) and for the complete signal (Δx) as a function of L. The focal width decreases as L increases and, for a given thickness, it is narrower at the second harmonic. $V_{in} = 285\,\mathrm{V}$ for each acquisition.

is repeated by exciting the transducer with applied voltages of 32 V and 158 V. In figure 7a, Δx is plotted against L for the three applied voltages. For $L = 8\,\mathrm{mm}$ the focal width decreases from 12 mm to 9.4 mm as the applied voltage is increased from 32 V to 285 V. When the slab is thicker this difference is less noticeable but, in general, the focal width tends to decrease as V_{in} increases. The explanation of this fact is delayed to the end of the section.

In figure 7b Δx_1 is plotted against L for the three voltages. There is no noticeable difference in the focal width as the applied voltage grows. The same behavior appears in the second harmonic. In figure 7c, Δx_2 is plotted against L only for voltages of 158 V and 285

V (at 32 V this harmonic is negligible). Again, the shift in the focal width as the applied voltage increases remains very small.

It is clear from the experiments that the behavior of the fundamental and the second harmonic do not depend of the applied voltage. Moreover, as happens in a linear regime[10], the focal width of both harmonics decreases to a limiting value if the thickness of the multiple scattering medium is increased. In addition, the focal width of the second harmonic is narrower than the focal width of the fundamental one, in connection to the better resolution given by a lower wavelength. These results are consistent with a decoupling between the

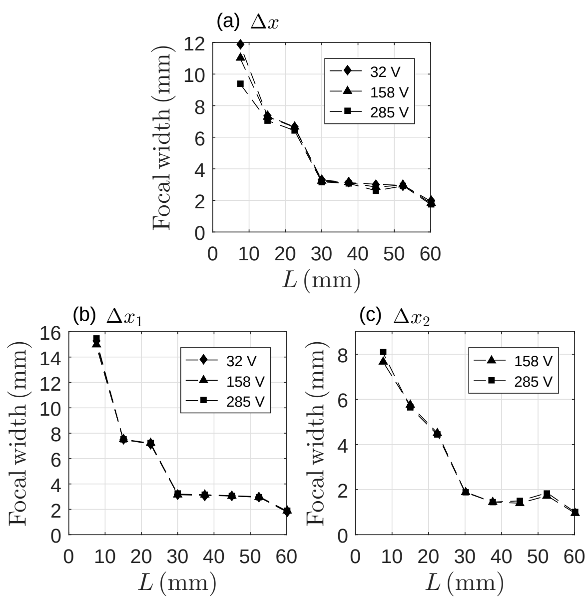

FIG. 7. -3 dB focal width of (a) the complete signal Δx, (b) the first harmonic Δx_1 and (c) the second harmonic Δx_2. At 32 V the amplitude of the second harmonic is very low so its focal width is not shown. For a given L, Δx decreases as V_{in} increases. This behavior is not seen on each harmonic separately.

scattering and the nonlinear phenomena but, before state a conclusion, the behavior of the whole wave and the time reversal process are analyzed with more detail.

Focusing by time reversal through a multiple scattering medium is possible due to the medium acting like an acoustic lens, whose effective aperture increases as its thickness do it so. This is because the multiple scattering allows to acquire components of the wavevector that, otherwise, would be lost to the sides[2]. In this way, and considering the multiple scattering medium as a lens with aperture D and focal length F, an estimation of the focal width can be given by:

$$\Delta x = \frac{\lambda F}{D} \tag{4}$$

where λ is an effective wavelength. Since there are at least two frequencies involved in the emission (the first and second harmonics) the effective wavelength can be calculated by performing the following weighted average:

$$\lambda = \sqrt{\alpha_1^2 \lambda_1^2 + \alpha_2^2 \lambda_2^2} \tag{5}$$

where $\lambda_1 = c_w/f_0$ is the wavelength associated with the central frequency and $\lambda_2 = c_w/2f_0$ the wavelength of the second harmonic. α_1 and α_2 are the weights of each frequency in the spectrum. This average is calculated in a discrete way, based on the work of J. Brum et al[15]. In equation 5 more harmonics can be included but they do not produce appreciable changes in the result. The relation 4 can be applied on the first harmonic, so that $\frac{F}{D} = \frac{\Delta x_1}{\lambda_1}$. Substituting this ratio in the equation 4 yields:

$$\Delta x = \frac{\lambda}{\lambda_1} \Delta x_1 \tag{6}$$

This substitution is reasonable as long as the thickness of the multiple scattering medium is larger than the mean free path and the F/D ratio is not related to the frequency nor the thickness of the slab. With the experimental values of α_1 and α_2 the value of λ was calculated. Together with the experimental value of Δx_1, Δx was calculated with the aid of equations 5 and 6. The result is shown in figure 8, where the experimental focal width and the estimated focal width of the whole signal are plotted against L ($V_{in} = 285\,\mathrm{V}$). Notice that, for $L > 30\,\mathrm{mm}$, the estimated values are very close to the experimental ones.

To show that the results are consistent, one more calculation is performed. The focal width reached is, in average, 2.7 mm for $L > 30\,\mathrm{mm}$, which yields an 1.4 mm effective wavelength. Using these values in equation 4, the F/D ratio yields 1.9. If $F = 250\,\mathrm{mm}$ is

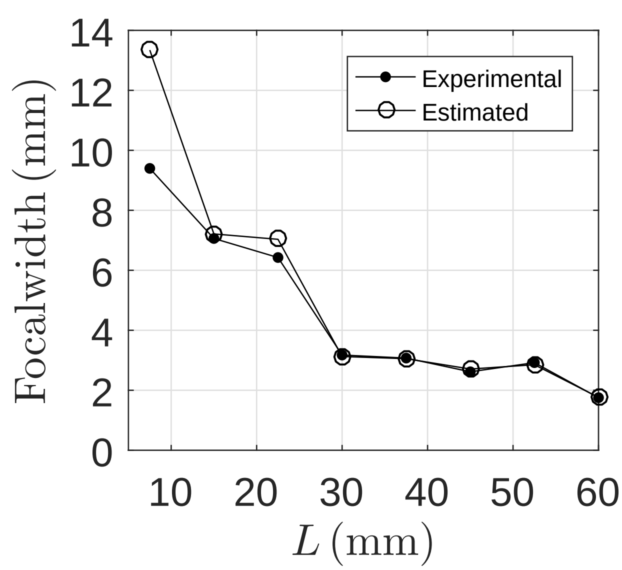

FIG. 8. Comparison between the experimental value of Δx ($V_{in} = 285\,\mathrm{V}$) and its estimation obtained by computing an effective wavelength. Both curves show a good agreement for $L >$ 30 mm.

assumed (distance between the transducer and the hydrophone), the slab can be considered as a lens of aperture $D = 132\,\mathrm{mm}$. This value is close to the length of the slab (140 mm on x-axis).

From the latter consideration, it can be explained why the focal width of the whole wave decreases as V_{in} is increased. As can be deduced from equation 5, the effective wavelength is smaller the more frequencies are present in the wave, which gives a lower focal width. Then, the nonlinear harmonics of the wave contribute to reduce the focal width. As a result, in a linear regime, the focal width should be greater than in a nonlinear regime.

Finally, the study of this section shows that the behavior of the whole wave together with the first and the second harmonic can be explained with elements of the linear theory. Then, we can assert that the wave propagates through the slab as in a linear regime.

VI. DISCUSSION

Throughout the work, it was presented evidence of the decoupling between the multiple scattering and the nonlinear phenomena for a particular system. This means that the propagation of the harmonics through the multiple scattering medium is essentially linear, despite a nonlinear phenomenon is required for the second harmonic to be generated. Under these conditions, it is possible to take advantage of the spectral richness of the nonlinear wave to study the response of a multiple scattering medium in a frequency range greater than that which can be covered in a linear regime.

The analysis leads to a new question: is there a condition on the emitted wave or in the slab construction where an interaction between nonlinear phenomena and multiple scattering can be observed? To answer this, two parameters must be considered: the amplitude of the emitted wave and the density of the multiple scattering medium. As was mentioned in III, these parameters are related to ϵ and η and the equation 1 is valid in conditions where $\eta\epsilon^2$ can be neglected. For $\eta\epsilon^2$ being in the order of η, the amplitude of the wave should be increased at least five orders of magnitude. This is not possible with the available amplification system. Then, equation 1 is a good model for the experiments proposed here. From this equation, it was suggested that the wave satisfies a linear scattering equation if ϵ^2 is negligible compared to η. For ϵ^2 to be of the same order of magnitude as η, the latter must be reduced by at least eight orders of magnitude. On one hand, this can be achieved by reducing the total area occupied by the scatterers by the same amount. One possibility is to dilute the medium by reducing the density of scatterers. However, the distance between them would be much greater than the wavelength and there would not be multiple scattering. As an alternative, the diameter of the scatters could be reduced at least four order of magnitude, but the construction of the slab would be impossible (at least in the way it was done in this work). On the other hand, copper could be replaced by another material. It is needed that the wave speed c_n of the new material be close to the wave speed in water. Precisely, their relative difference $\left|\frac{c_n - c_w}{c_w}\right|$ must be in the order of 10^{-8}. Although the experiments presented in this work were performed in specific conditions, based on the orders of magnitude computed above, it can be concluded that multiple scattering phenomena will not interact with nonlinear phenomena in a wide range of conditions. In a future work, the possibility of achieving an interaction between multiple scattering and nonlinear phenomena will be investigated attempting to find a different scattering medium.

VII. CONCLUSION

It has been shown that the time reversal focusing improves if the thickness of the multiple scattering medium increases. The results reported here show that this is true even for nonlinear waves. This fact is consistent with an absence of interaction between nonlinear and multiple scattering phenomena and it suggests the possibility of using the virtual time reversal focusing technique as a coupling test between these phenomena.

The nonlinear propagation introduces higher frequencies into the wave spectrum. Based on the behavior of the first and second harmonics two conclusions can be pointed out:

a) the expansion of frequency components of the wave improves the quality of focusing by time reversal;

b) the focal width of the second harmonic is narrower than the focal width of the fundamental. Therefore, by taking advantage of the second harmonic in a time reversal process, it is possible to obtain resolutions below the value of the central wavelength.

In this work, focusing by virtual time reversal of nonlinear waves was studied. The results reported may eventually not agree with a real time reversal experiment. However, in conditions where the nonlinear effects are decoupled from the multiple scattering effects, the harmonics propagate independently from each other, obeying a linear wave equation. Therefore, it is expected that the wave focusing of a real time reversal experiment agree with the results reported here.

ACKNOWLEDGMENTS

This work was supported by Agencia Nacional de Investigación e Innovación (ANII) under the grant FCE_1_2017_1_135582. The authors also thank to Comisión Académica de Posgrado (CAP) and CSIC for supporting the project Laboratorio de Acústica Ultrasonora.

REFERENCES

[1]M. Silk and B. Lidington, “The potential of scattered or diffracted ultrasound in the determination of crack depth,” Non-Destructive Testing **8**(3), 146–151 (1975).

[2]A. Derode, A. Tourin, and M. Fink, “Random multiple scattering of ultrasound. i. coherent and ballistic waves,” Physical Review E **64**(3), 036605 (2001).

[3]A. Tourin, A. Derode, A. Peyre, and M. Fink, “Transport parameters for an ultrasonic pulsed wave propagating in a multiple scattering medium,” The Journal of the Acoustical Society of America **108**(2), 503–512 (2000).

[4]N. Viard, B. Giammarinaro, A. Derode, and C. Barriere, “Coherent transmission of an ultrasonic shock wave through a multiple scattering medium,” Physical Review E **88**(2), 023201 (2013).

[5]M. Fink, “Time reversal of ultrasonic fields. i. basic principles,” IEEE transactions on ultrasonics, ferroelectrics, and frequency control **39**(5), 555–566 (1992).

[6]F. Wu, J.-L. Thomas, and M. Fink, “Time reversal of ultrasonic fields. il. experimental results,” IEEE transactions on ultrasonics, ferroelectrics, and frequency control **39**(5), 567–578 (1992).

[7]G. Montaldo, P. Roux, A. Derode, C. Negreira, and M. Fink, "Generation of very high pressure pulses with 1-bit time reversal in a solid waveguide," The Journal of the Acoustical Society of America **110**(6), 2849–2857 (2001).

[8]B. Arnal, M. Pernot, M. Fink, and M. Tanter, "Tunable time-reversal cavity for high-pressure ultrasonic pulses generation: A tradeoff between transmission and time compression," Applied Physics Letters **101**(6), 064104 (2012).

[9]J. Robin, B. Arnal, M. Tanter, and M. Pernot, "A 3d time reversal cavity for the focusing of high-intensity ultrasound pulses over a large volume," Physics in Medicine & Biology **62**(3), 810 (2017).

[10]A. Derode, A. Tourin, and M. Fink, "Random multiple scattering of ultrasound. ii. is time reversal a self-averaging process?," Physical Review E **64**(3), 036606 (2001).

[11]M. Tanter, J.-L. Thomas, F. Coulouvrat, and M. Fink, "Breaking of time reversal invariance in nonlinear acoustics," Physical review E **64**(1), 016602 (2001).

[12]T. L. Szabo, *Diagnostic ultrasound imaging: inside out* (Academic Press, 2004).

[13]F. Dagrau, M. Rénier, R. Marchiano, and F. Coulouvrat, "Acoustic shock wave propagation in a heterogeneous medium: A numerical simulation beyond the parabolic approximation," The Journal of the Acoustical Society of America **130**(1), 20–32 (2011).

[14]N. Benech, S. Catheline, J. Brum, T. Gallot, and C. A. Negreira, "1-d elasticity assessment in soft solids from shear wave correlation: The time-reversal approach," IEEE transactions on ultrasonics, ferroelectrics, and frequency control **56**(11), 2400–2410 (2009).

[15] J. Brum, S. Catheline, N. Benech, and C. Negreira, "Quantitative shear elasticity imaging from a complex elastic wavefield in soft solids with application to passive elastography," IEEE transactions on ultrasonics, ferroelectrics, and frequency control **62**(4), 673–685 (2015).